KEK--92-4

JP9301164

KEK Report 92-4
May 1992
A

Evaluation of Ring Impedance of the Photon Factory Storage Ring

T. KIUCHI, M. IZAWA, S. TOKUMOTO, Y. HORI, S. SAKANAKA,
M. KOBAYASHI and H. KOBAYAKAWA

NATIONAL LABORATORY FOR
HIGH ENERGY PHYSICS

KEK Reports are available from:

Technical Information & Library
National Laboratory for High Energy Physics
1-1 Oho, Tsukuba-shi
Ibaraki-ken, 305
JAPAN

Phone: 0298-64-1171
Telex: 3652-534 (Domestic)
(0)3652-534 (International)
Fax: 0298-64-4604
Cable: KEKOHO

EVALUATION OF RING IMPEDANCE OF THE PHOTON FACTORY STORAGE RING

T. Kiuchi*, M. Izawa, S. Tokumoto, Y. Hori, S. Sakanaka,
M. Kobayashi and H. Kobayakawa

National Laboratory for High Energy Physics
Oho 1-1, Thukuba-shi, IBARAKI, 305 Japan
*Fujitsu Laboratories Ltd. Atsugi

Abstract

The loss parameters of the ducts in the Photon Factory (PF) storage ring were evaluated using the wire method and the code TBCI. Both the measurement and the calculation were done for a different bunch length (σ) ranging from 23 to 80 ps.

The PF ring impedance was estimated to be $|Z/n|=3.2\ \Omega$ using the broadband impedance model. The major contribution to the impedance comes from the bellows and the gate valve sections. Improvements of these components will lower the ring impedance by half.

1. Introduction

The PF ring is a 2.5 GeV positron storage ring dedicated to synchrotron radiation applications. The start current in the multi-bunch user run exceeds 350 mA with the beam lifetime of more than 60 hours. Recently, the single bunch operation for user's experiments started, however, the stored current is restricted to about 35 mA because of the poor lifetime due to the vacuum deterioration caused by the local heating of some chambers. It is apparent that such local heating is caused by the parasitic loss of the single bunch beam. Besides such problem, the bunch lengthening and the instability were also observed. These phenomena are closely concerned with the broadband impedance of the ring. We then started, at first, to evaluate the loss parameter of each component in the PF ring. Although the loss parameter is related to only the real part of the impedance, it is an important parameter which provides us with a view of the ring impedance.

The loss parameters were measured or calculated at several bunch lengths, ranging 23 to 80 ps. Generally, the impedance of each component becomes resistive in the short bunch region, so that the loss parameter becomes large as the bunch length becomes short. However, its dependence on the bunch length is different for each component. The results of this study will show us what kind of duct components we should avoid using.

On the other hand, from the total loss parameter and its dependence on the bunch length, the broadband impedance of the ring can be estimated under certain assumptions. By supposing the ring has a single low-Q (=1) resonance at around the cutoff

frequency of the duct, the PF ring impedance was estimated to be $|Z/n|=3.2\ \Omega$.

2. Duct Components in the PF Ring

The PF ring duct components are listed in Table 1. The duct components studied in this paper are as follows:

(1) Quadrupole magnet duct

The duct for the quadrupole magnet is referred to as the Q-duct. There are three types of the Q-ducts: (a) the Q-duct made of stainless steel(the SS Q-duct), (b) that of Aluminum(the Al Q-duct) and (c) the Q-duct for the new quadrupole magnet (the Q_a-duct) which was installed in 1987 to realize the present low-emittance operation; their cross sections are shown in Fig.1.

The Q-duct components that we examined are the bellows, pumping port and flange gap which have the same cross section as the SS Q-duct, and also, the position monitor and SR absorber that are mounted in the SS Q-duct. They are made of stainless steel. These components are indicated by "Q-" such as Q-Bellows, Q-Single Port, Q-Double port (pumping port), Q-Abs (absorber) and Q-FG (flange gap).

(2) Round duct

The round duct (R-duct) is mainly used in RF accelerating cavity sections. The duct components which have round cross section are shown by "R-" such as R-FG (flange), R-Bellows and R-Abs (absorber).

Many tapered ducts are used for Q-duct to/from B-duct (the duct for the bending magnet) , Q-duct to/from R-duct and for the

insertion device chambers. Most of these transitions were ignored in this study, since they have very smooth tapers. However, several exceptions were taken into account and are shown in Table 1.

The B-duct and the ceramic ducts used in the kicker and RFQ magnet were not taken into account. The contribution of these ducts to the ring impedance would be the main subject after improving the ducts studied in this paper.

The loss parameter of each component was obtained by using the wire method[1,2,3] or by the numerical calculation (TBCI[4]). The methods of evaluating each component are also listed in Table 1.

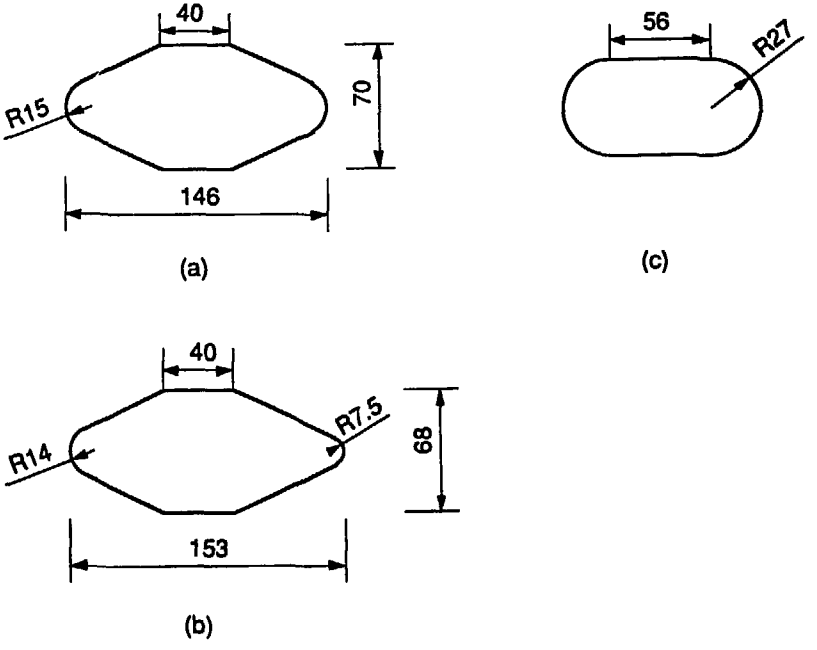

Fig. 1 Cross-sectional view of the Q-duct.
(a): the SS Q-duct, (b): the Al Q-duct, (c): the Q_a-duct.

Table 1 List of PF ring components.

Component	Quantity	Description	Method of Evaluation
RF Cavity	4	Ref. 1	Calculation
Flange Gap			
Q-FG#1	20	Q-duct & ICF203 Gap 1 mm	Measured
Q-FG#2	39	Q-duct & ICF203 Gap 3 mm	Measured
R-FG#1	8	R-duct ϕ100 & ICF203 Gap 21 mm	Meas. & Calculation
Bellows			
R-Bellows#1	1		Calculation
R-Bellows#2	1		Calculation
R-Bellows#3	1		Calculation
R-Bellows#4	2		Calculation
R-Bellows#5	2		Calculation
R-Bellows#6	1		Calculation
R-Bellows#7	1		Calculation
R-Bellows#8	1		Calculation
R-Bellows#9	1		Calculation
Q-Bellows	98	Bellows installed at Q-duct	Measured
Pumping port			
Q-Single Port	11		Measured
Q-Double Port	33		Measured
SR Absorber			
Q-Abs35mm	1	35 mm from Beam Center	Measured
Q-Abs43mm	2	43 mm from Beam Center	Interpolation
Q-Abs47mm	8	47 mm from Beam Center	Interpolation
Q-Abs58mm	6	58 mm from Beam Center	Interpolation
Q-Abs59mm	2	59 mm from Beam Center	Interpolation
Q-Abs60mm	5	60 mm from Beam Center	Interpolation
Q-Abs61mm	5	61 mm from Beam Center	Interpolation
Q-Abs62mm	4	62 mm from Beam Center	Interpolation
Q-Abs63mm	2	63 mm from Beam Center	Interpolation
Q-Abs64mm	1	64 mm from Beam Center	Interpolation
Q-Abs66mm	4	66 mm from Beam Center	Interpolation
Q-Abs67mm	2	67 mm from Beam Center	Interpolation
Q-Abs68mm	2	68 mm from Beam Center	Interpolation
Q-Abs69mm	2	69 mm from Beam Center	Interpolation
R-Abs17mm	1	17 mm from Beam Center	Interpolation
R-Abs36mm	1	36 mm from Beam Center	Interpolation
R-Abs38mm	1	38 mm from Beam Center	Interpolation
R-Abs41mm	1	41 mm from Beam Center	Interpolation
R-Abs46mm	1	46 mm from Beam Center	Interpolation
R-Abs50mm	1	50 mm from Beam Center	Interpolation

continued on the next page

Component	Quantity	Description	Method of Evaluation
Gate Valve			
GV#2	2	Upstream of RF cavity	Calculation
GV#3	1	Downstream of RF cavity	Calculation
GV#4	1	Downstream of RF cavity	Calculation
GV#5	1	Upstream of Undulator #2	Calculation
GV#6	1	Upstream of wall current monitor	Calculation
GV#7	1	Upstream of VW#14	Calculation
GV#11	2	Downstream of B19	Calculation
GV#12	2	DCCT and RCT	Calculation
GV#13	1	Upstream of B13	Calculation
GV#14	1	Upstream of septum magnet	Calculation
GV#17	2	RF shielded valve & matched radius	Ignored
Taper Transition			
TP#1	1	RFKO & downstream of VW#14	Calculation
TP#3	1	RFQ	Calculation
TP#4	2	Qa - Al Q duct	Calculation
TP#5	2	Octupole Duct type A	Calculation
TP#6	6	Octupole Duct type B	Calculation
Position Monitor	45	Button type beam position monitor	Measured

3. Measurement Set-up

As mentioned in the introduction, the loss parameters of the components were measured using the wire method. Measurements were carried out in the frequency domain using a network analyzer (HP 8510B). In this section we describe our measurement set-up and some results of assessing the data validity.

Figure 2 shows the measurement set-up for the frequency domain. The frequency domain data were converted to the time domain via FFT to obtain synthetic pulses. The loss parameters were then calculated using these pulses. The synthetic pulses obtained from our measurements had close-to-Gaussian shapes. Their standard deviation (σ) ranged from 23.1 to 78.3 ps.

As noted in reference 3, measurements in the frequency domain have the advantage of a higher spectral power density than those in the time domain. They, thus, have a higher dynamic range and better reproducibility. However, there are some ambiguities in calculating synthetic pulses from the frequency domain data via FFT. The results are restricted by an equidistant

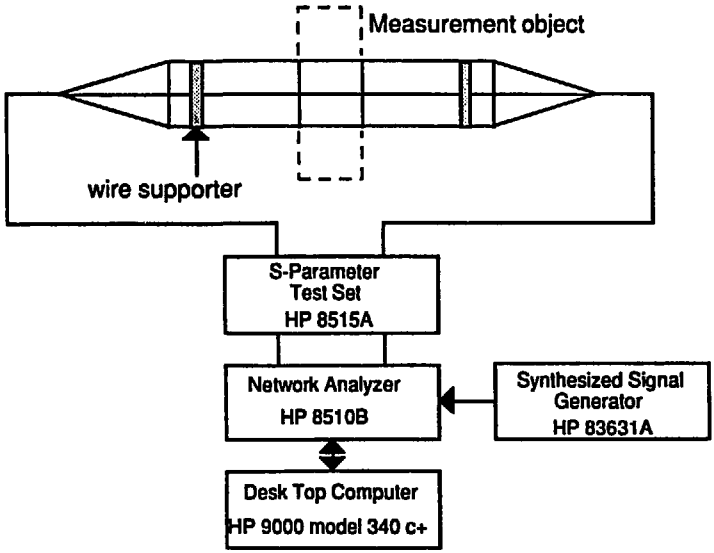

Fig. 2 Measurement set-up

sampling problem[5] and the ambiguity of evaluating the DC component. The validity of the data obtained from frequency domain measurements will be discussed later.

The test section comprised two taper transitions, two straight sections, a reference duct or measurement object, inner wire and two inner wire supporters. The taper transition is the impedance-matching section. Figure 3 shows a draft of the taper transitions. The taper transition has a PC-7 microwave connector

at the end, and the inner wire is 3.0 mm in diameter. The PC-7 connector at the end of taper transitions enabled us to remove impedance mismatching in the connections to 50 Ω cable. The straight sections were 514 mm long for Q-duct measurements and 420 mm long for R-duct measurements. These were sufficiently long to eliminate the effect of multiple reflections. Two styrol foam supports were placed in the straight sections to prevent inner wire sagging.

The room temperature variation was kept within ±0.1 °C.

Typical synthetic pulses for round bellows measurements are shown in Fig. 4.

To evaluate the loss parameter (k), we used the following equations: [1,2,3]

$$k(\sigma) = \frac{2Z_0}{Q^2}\int I_0(t)I_S(t)dt. \qquad (1)$$

Here,

$Q = \int I_0(t)dt$: charge in the pulse,

$I_0(t)$: reference pulse,

$I_m(t)$: measured pulse modified by the measurement object,

$I_S(t) = I_0(t) - I_m(t)$: subtracted signal,

Z_0 : characteristic impedance of the coaxial line formed by the reference duct and the wire,

σ : standard deviation of the Gaussian pulse.

The measured pulse $I_m(t)$ was time-shifted so that the first 10-20% of the pulse coincided with the reference pulse $I_0(t)$. The

limits of the integral in Eq. (1) were from t-2σ to t+2σ (t is the mean value of the Gaussian pulse) to avoid the multiple reflections.

The characteristic impedance (Z_0) of a Q-duct with an inner wire of 3.0 mm diameter was calculated by the code POISSON.[6] The result was Z_0= 203.81 Ω. To assess its accuracy, we calculated the characteristic impedance of a coaxial symmetric air line.

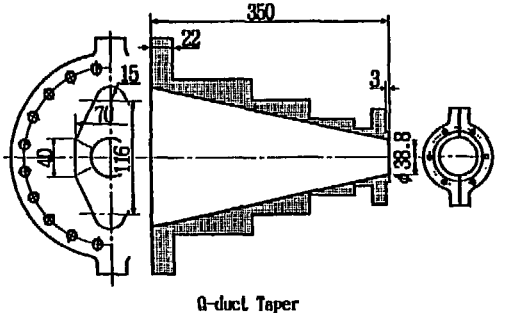

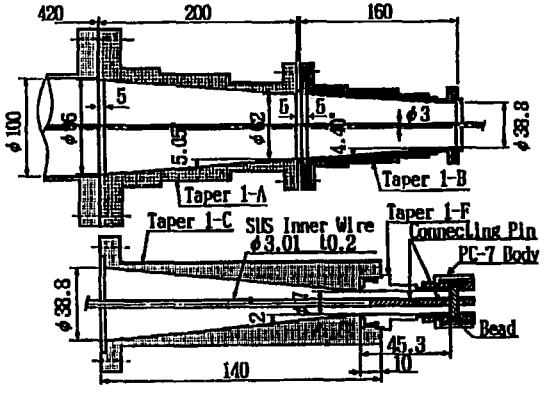

Fig. 3 Draft of Taper transitions

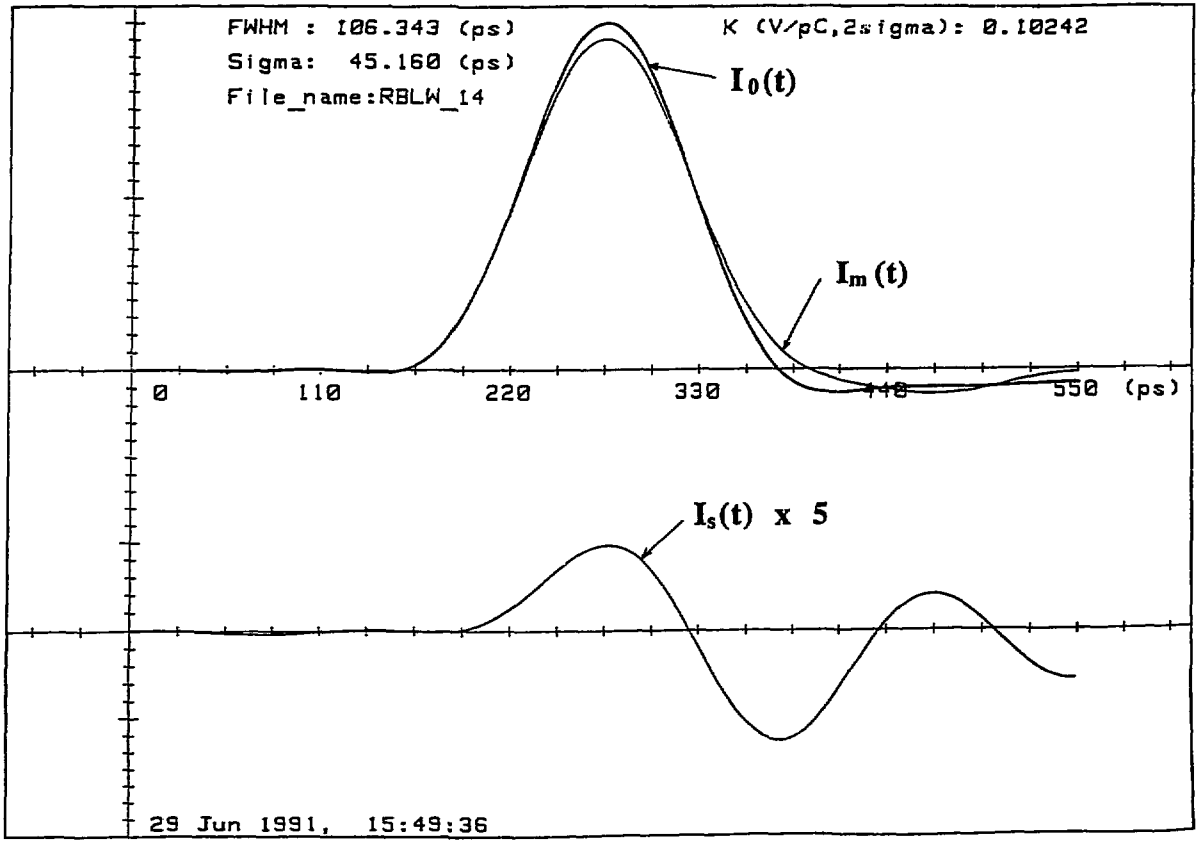

Fig. 4 Typical synthetic pulses for round bellows measurements.

The diameter of an inner conductor is 3.0 mm and that of an outer conductor is 100.0 mm. The characteristic impedance given by POISSON was 214.12 Ω, compared with 210.25 Ω by analytic calculations. The accuracy in this case was 1.84%; that for the Q-duct is considered to be similar. The characteristic impedance of the Q-duct with an inner wire of 3.0 mm diameter is, therefore, $Z_0 = 204 \pm 4\ \Omega$.

The R-duct has a diameter of 100.0 mm. Therefore, the characteristic impedance (Z_0) of the R-duct is $Z_0 = 210.25\ \Omega$

Before we examined the Q-duct components with a three-dimensional structure, we examined the RF accelerating cavity[7] and a round bellows. This checked the validity of the measuring systems and allowed us to evaluate the accuracy of obtained data. Since the RF accelerating cavity and the round bellows both have a cylindrically symmetric structure, TBCI can be used without any simplification. The dimensions of the bellows are shown in Fig. 5.

Figure 6 compares the measured data in the frequency domain and the results calculated by TBCI for the RF accelerating cavity. The agreements are quite good.

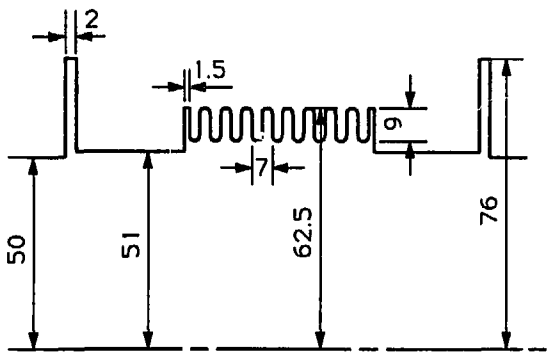

Fig. 5 Dimension of the round bellows

Figure 7 compares the measured data in the frequency domain and the calculated results for the round bellows. The measured data in the frequency domain and the calculated results agree closely.

The overall resolution of the measured loss parameters is less than 0.01 V/pC.

4. Results of Measurements

I. RF accelerating cavity

The results for the RF accelerating cavity mentioned in the previous section include the fundamental mode-loss parameter (k_0). The fundamental mode loss parameter (k_0), given by the following equation, is calculated by the program URMEL:[8]

$$k_0(\sigma) = (\omega_0/4)(R/Q)_0 \exp(-\omega_0^2\sigma^2) . \qquad (2)$$

The value of $k_0(\sigma)$ is almost constant for σ from 20 to 100 ps and is 0.176 V/pC. The cavity fundamental loss parameter (k_0) is ignored when evaluating the ring impedance in the following section.

II. Q-bellows

A typical Q-bellows is shown in Appendix. There are about one hundred Q-bellows in the ring. Their length is slightly different from the typical Q-bellows, depending on the location where they are used. However, the small difference in the length is ignored in this study. The total loss parameter of the Q-bellows was obtained by multiplying the measured loss parameter shown in Fig. 8 by the number of the Q-bellows.

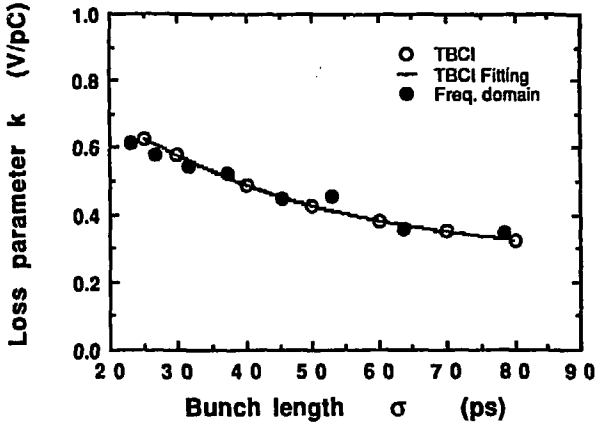

Fig. 6 Comparison of the measured and calculated results for an RF accelerating cavity.

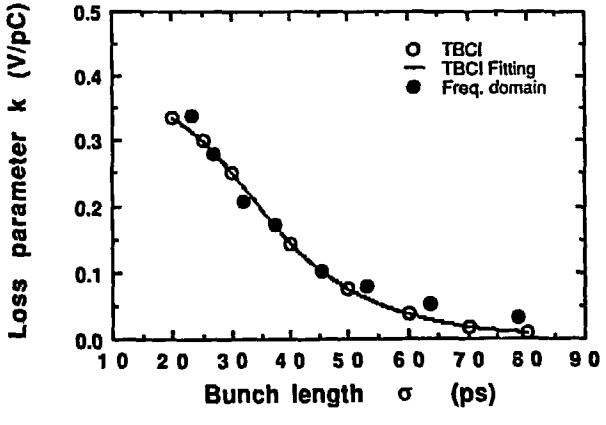

Fig. 7 Comparison of the measured and calculated results for round bellows.

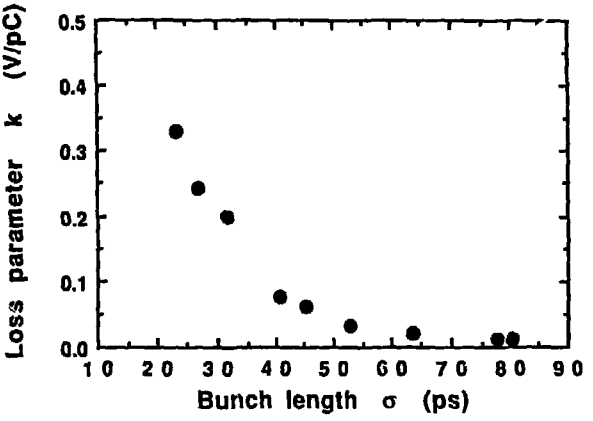

Fig. 8 Loss parameter of the Q-bellows

III. Round duct pumping chamber

A round duct pumping chamber is an assembly comprising a large conductance chamber and pumps. The chamber has a ϕ150 (mm) round duct with slits-holes that are designed to separate electromagnetically part of the beam duct from the pumping section, as is shown in appendix. The loss parameter is measured with a ϕ100 (mm) straight pipe connected at each side. The results are shown in Fig. 9. We also calculated the loss parameter for the ϕ150 (mm) round duct without slits-holes using TBCI; the results are also shown in Fig. 9. Since the difference between the measured and calculated data was very small, we concluded that the slits-holes act as a good RF shield. Therefore, the contribution of slits-holes to the loss parameter is ignored in this study.

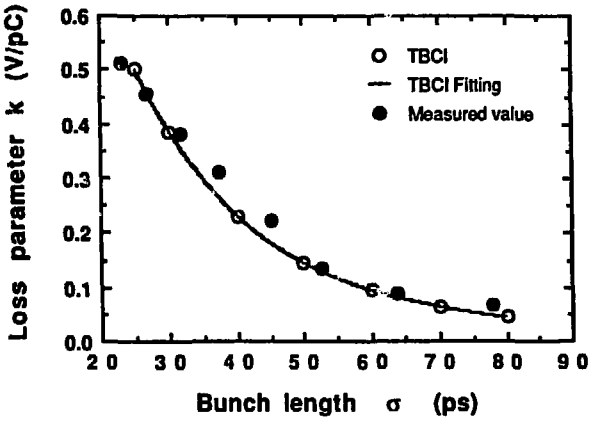

Fig. 9 Loss parameter of an R-duct pumping port

IV. SR Absorber

SR absorbers[9] are of two types: those installed in a Q-duct (shown in Appendix), and those installed in an R-duct. We have examined the absorbers in a Q-duct. The results are shown in Fig.10 as a function of the inserted length of the absorber measured from the beam duct center. The inserted lengths of absorbers actually measured are 17, 25, 30, 35, 40, 45, 50, 55 and 70 mm. The loss parameter of the absorbers listed in Table 1 are interpolated form the measured data. We assume that the loss parameter of an absorber in an R-duct is the same as that of an absorber in a Q-duct.

V. Q-duct flange gap

The loss parameters of Q-duct flange gaps of 1, 2, 3, 4, 5 and 8 mm length were measured. The results are shown in Fig. 11. The

Q-duct flange gap widths actually used in the ring are 1 mm and 3 mm.

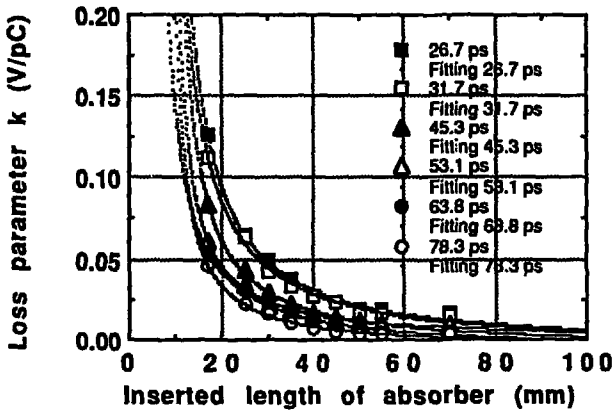

Fig. 10 Loss parameter of the Q-duct SR absober. Inserted lengths were measured from the beam duct center

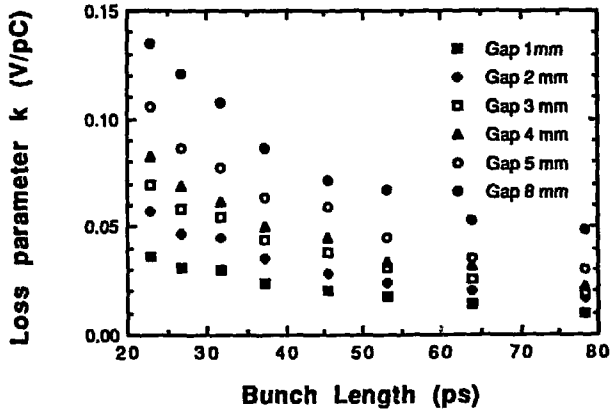

Fig. 11 Loss parameter of the Q-duct flange gap

VI. Position monitor

There are 45 position monitors in the PF ring. Each position monitor comprises 6 disk-shaped electrostatic electrodes that are directly mounted in the Q-duct. Each 29 mm diameter electrode is enclosed in the housing with a vacuum tight connector. Each electrode was terminated by a 50 Ω load during measurement. The measured loss parameter of a position monitor is shown in Fig. 12.

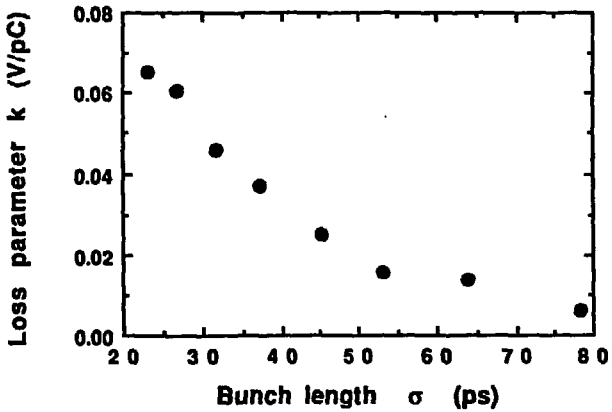

Fig. 12 Loss parameter of position monitor.

5. Numerical calculations

The loss parameter of the components having a round or close to round cross section were calculated using TBCI. When they have a three-dimensional cross section as a part, we simplified them into a two-dimensional cylindrically symmetric model. The TBCI calculation was carried out for bunch lengths of 25, 30, 40, 50, 60, 70 and 80 ps. The loss parameters at other

bunch lengths were obtained by an interpolation using the spline function of order three.

The flange gap with R-duct and the round bellows have cylindrical symmetry. Their loss parameters were calculated using TBCI without any approximation.

Three kinds of gate valves are used in the PF ring: the first has no RF shield; the second has an RF shield, but has a step change in cross section at the connection with the duct; the third has an RF shield and no step change. The third ones can be ignored from the impedance point of view. The first and second type gate valves are assembled into 12 gate valve sections, which are composed of some other components such as taper transitions, DCCT, RCT, etc. These gate valve sections are shown in Appendix as GV#2 to GV#14. We simplified these gate valve sections into a two-dimensional cylindrically symmetric structure and calculated their loss parameters using TBCI. As shown in the appendix, some gate valve sections have the Q-duct. In a calculation, the Q-duct was simplified into a vertically inscribed cylinder, as is shown in Fig. 13.

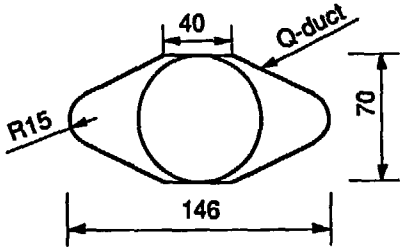

Fig. 13 Cross-sectional view of a vertically inscribed cylinder in Q-duct

To check the validity of this simplification, we measured the loss parameter of a round gap with Q-ducts, which is shown in Appendix as GV#16, and compared it with the results of TBCI. Figure 14 compares the calculated values (k(σ)) with the measured values. The agreement is quite good.

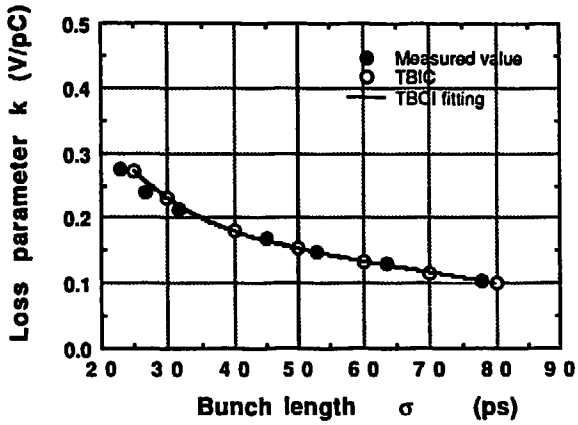

Fig. 14 Comparison of the GV#16 loss parameter calculated and measured.

There are a lot of taper transitions in the PF ring. Among these transitions, we examined 5 types of taper transitions, since their corss sections greatly change. These transitions are shown in Appendix as TP#1 and TP#3 to TP#6. In a calculation, we simplified the Q-duct into inscribed cylinder. In the case of TP#5, we used a horizontally circumscribed cylinder to simplify this structure, since the horizontal dimension changes more than does that of the vertical.

The results of numerical calculations are summarized below.

I. Round flange gap

As mentioned above, since this component has a two-dimensional cylindrically symmetric structure, TBCI can be used without any simplified modeling. The results are shown in Fig. 15.

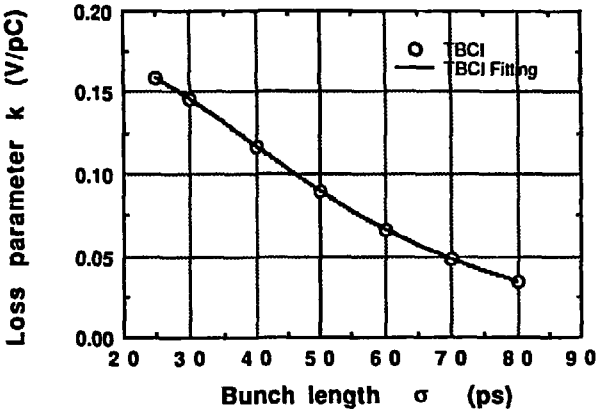

Fig. 15 Loss parameter of a round flange gap (R-FG#1)

II. Round bellows

The round bellows are shown in Appendix as R-bellows#1 to R-bellows#9. Since these components have a two-dimensional cylindrically symmetric structure, TBCI can again be used without any simplified modeling. The results are shown in Fig. 16.

III. Gate valve sections

The gate valve sections are shown in appendix as GV#1 to GV#7 and GV#11 to GV#16. Gate valves GV#1 and GV#16 are not actually used in the ring. The results are shown in Fig. 17 (a) for GV#2 to GV#7 and in Fig. 17(b) for GV#11 to GV#15.

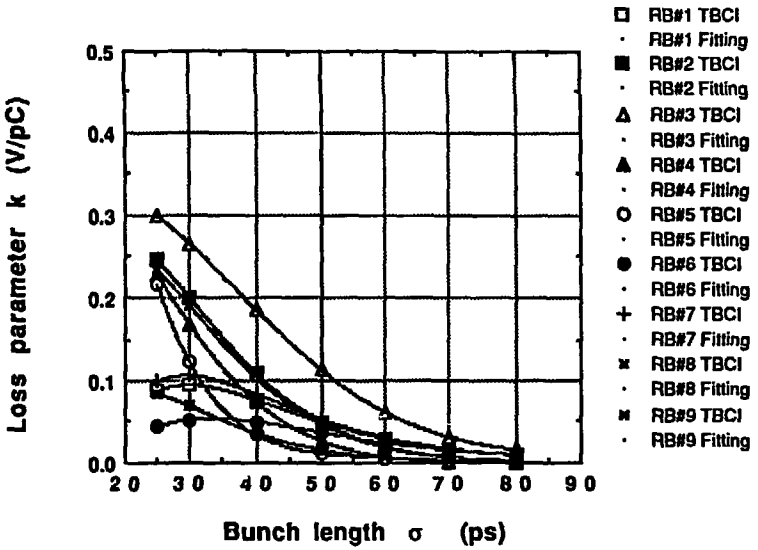

Fig. 16 Loss parameter of a round bellows (R-B#1 to R-B#9).

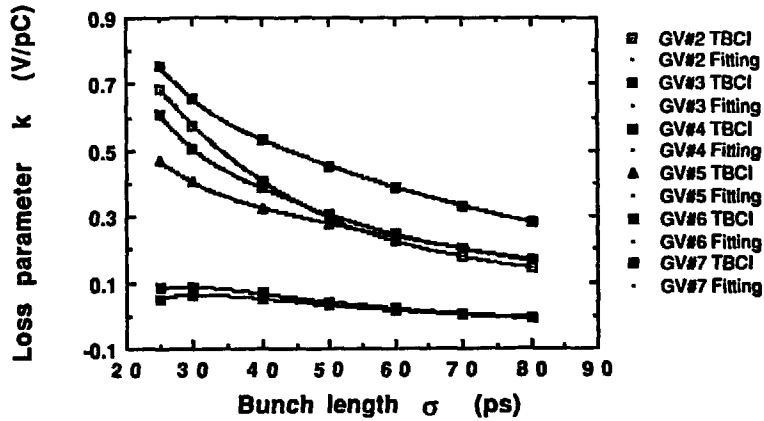

Fig. 17 (a) Loss parameters of gate valves

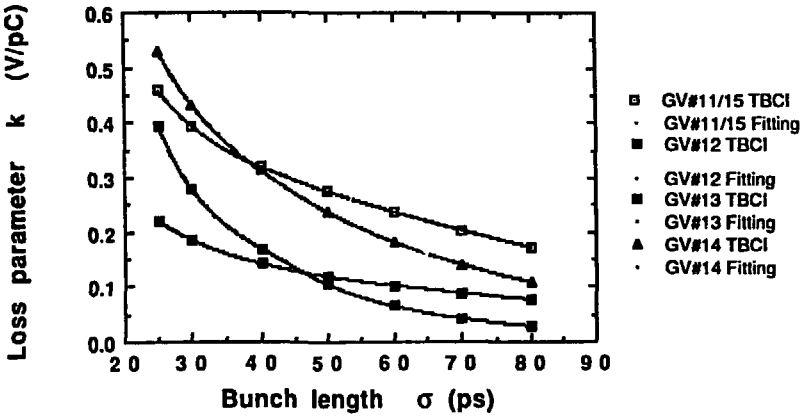

Fig. 17 (b) Loss parameters of gate valves.

IV. Taper transitions

The Taper transitions examined in this study are shown in Appendix as TP#1 and TP#3 to TP#6. Figure 18 shows the results.

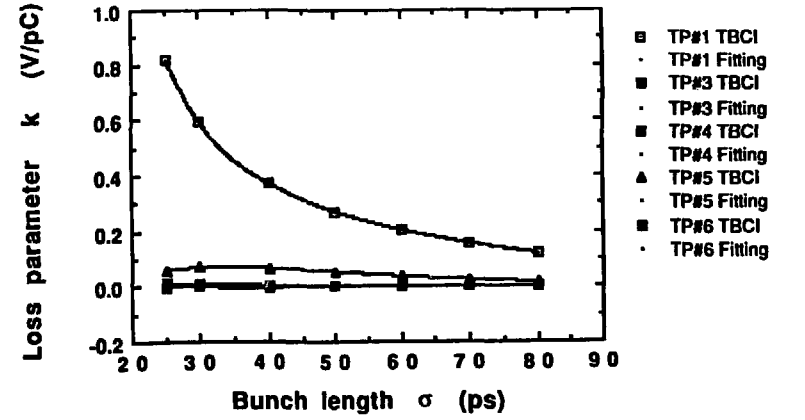

Fig.18 Loss parameters of taper transitions

6. Parasitic Energy Loss and Ring Impedance

In order to obtain the total loss parameters of the PF ring, the measured and the calculated loss parameters were added at the bunch lengths of 26.7 , 31.7 , 45.2 , 53.0 , 63.6 and 78.3 ps. The results are summarized in Table 2.

From Table 2, one can evaluate the parasitic energy loss in the components. The natural bunch length of the PF ring is 50 ps. We evaluate the parasitic energy loss for a bunch length (σ) of 53.0 ps, though this length is slightly greater than that of the PF ring. Table 6-2 summarizes the power loss in the components having large loss parameters for a bunch length of σ= 53.0 ps, and, a beam current (I_0) of 50 mA. We used the following formula[10] to evaluate the power loss in the components:

$$P = I_0^2 \, k \, T_b \, . \qquad (3)$$

Here,

I_0 : average beam current,

k : loss parameter,

T_b : interval between bunches.

As shown in Table 3, the components which have a large energy loss are gate valves.

The ring impedance was evaluated using the broad band impedance model.[11]

The broad band impedance is given by the following equation:

$$Z(\omega) = \frac{R_S}{1+jQ(\frac{\omega}{\omega_c} - \frac{\omega_c}{\omega})} \qquad (4)$$

Here,

R_S : shunt impedance,

ω_c : resonance frequency,

Q : quality factor.

The value of the quality factor (Q) is fixed at 1 in this study. The relationship between the ring impedance ($Z(\omega)$) and the total loss parameter (K) is given by the following equation,[12] assuming a Gaussian bunch:

$$K(\sigma) = \frac{1}{\pi}\int_0^\infty Re(Z(\omega))\exp(-\omega^2\sigma^2)d\omega \,. \qquad (5)$$

Here,

σ : standard deviation of Gaussian bunch.

Substituting Eq. (4) in Eq. (5), we obtain

$$K(\sigma) = \frac{1}{\pi}\int_0^\infty \frac{R_S\exp(-\omega^2\sigma^2)}{1+(\frac{\omega}{\omega_c} - \frac{\omega_c}{\omega})^2} d\omega \,. \qquad (6)$$

The parameter $|Z/n|$, generally called the "broad band impedance", is defined as

$$|Z/n| = R_S\frac{\omega_0}{\omega_c} \,, \qquad (7)$$

where

ω_0 : revolution angular frequency,

ω_c : resonance frequency.

Table 2 List of loss parameters of ring components.

Component	Quantity	Bunch length 26.7 ps	31.7 ps	45.2 ps	53.0 ps	63.6 ps	78.3 ps
		Total k (V/pC)					
RF Cavity *	4	1.612	1.472	1.100	1.100	0.793	0.679
Flange Gap							
Q-Q 1mm	20	0.700	0.640	0.440	0.400	0.320	0.220
Q-Q 3mm	39	2.262	2.145	1.482	1.209	0.975	0.780
R-R ϕ100	8	1.238	1.129	0.818	0.657	0.474	0.293
		4.20	3.914	2.740	2.266	1.769	1.293
Bellows							
R-Bellows#1	1	0.092	0.094	0.062	0.042	0.023	0.010
R-Bellows#2	1	0.231	0.184	0.074	0.038	0.014	0.003
R-Bellows#3	1	0.289	0.253	0.146	0.095	0.048	0.017
R-Bellows#4	2	0.414	0.298	0.089	0.037	0.008	-0.002
R-Bellows#5	2	0.359	0.198	0.036	0.018	0.009	0.003
R-Bellows#6	1	0.048	0.053	0.043	0.033	0.021	0.011
R-Bellows#7	1	0.104	0.105	0.067	0.045	0.025	0.010
R-Bellows#8	1	0.220	0.175	0.070	0.036	0.013	0.003
R-Bellows#9	1	0.080	0.063	0.023	0.012	0.004	0.000
Q-Bellows	98	23.699	19.550	5.876	3.122	2.071	1.148
		25.536	20.973	6.486	3.478	2.236	1.203
SR Absorber							
Q-Abs35mm	1	0.038	0.035	0.023	0.019	0.016	0.011
Q-Abs43mm	2	0.054	0.051	0.031	0.029	0.022	0.014
Q-Abs47mm	8	0.189	0.175	0.106	0.102	0.072	0.046
Q-Abs58mm	6	0.101	0.092	0.052	0.058	0.032	0.018
Q-Abs59mm	2	0.033	0.030	0.017	0.019	0.010	0.006
Q-Abs60mm	5	0.079	0.072	0.041	0.046	0.024	0.013
Q-Abs61mm	5	0.077	0.070	0.039	0.045	0.023	0.013
Q-Abs62mm	4	0.060	0.054	0.030	0.035	0.017	0.009
Q-Abs63mm	2	0.029	0.026	0.015	0.017	0.008	0.004
Q-Abs64mm	1	0.014	0.013	0.007	0.008	0.004	0.002
Q-Abs66mm	4	0.054	0.048	0.026	0.032	0.014	0.004
Q-Abs67mm	2	0.026	0.023	0.013	0.016	0.007	0.003
Q-Abs68mm	2	0.025	0.023	0.012	0.016	0.006	0.003
Q-Abs69mm	2	0.025	0.022	0.012	0.015	0.006	0.003
R-Abs17mm	1	0.126	0.113	0.084	0.061	0.054	0.046
R-Abs36mm	1	0.036	0.033	0.021	0.018	0.015	0.010
R-Abs38mm	1	0.033	0.031	0.019	0.017	0.014	0.009
R-Abs41mm	1	0.029	0.027	0.017	0.015	0.012	0.008
R-Abs46mm	1	0.024	0.023	0.014	0.013	0.009	0.006
R-Abs50mm	1	0.021	0.020	0.012	0.012	0.008	0.005
		1.073	0.981	0.591	0.593	0.373	0.233

*Not included K_0=0.176

continued on the next page

Component	Quantity	Bunch length 26.7 ps	31.7 ps	45.2 ps	53.0 ps	63.6 ps	78.3 ps
		Total k (V/pC)					
Gate Valve							
GV#2	2	1.296	1.087	0.689	0.544	0.413	0.300
GV#3	1	0.058	0.063	0.041	0.027	0.011	-0.005
GV#4	1	0.087	0.085	0.053	0.036	0.017	-0.002
GV#5	1	0.445	0.386	0.301	0.267	0.226	0.175
GV#6	1	0.570	0.478	0.342	0.286	0.229	0.171
GV#7	1	0.717	0.627	0.491	0.434	0.368	0.292
GV#11/#15	2	0.868	0.754	0.590	0.526	0.450	0.354
GV#12	2	0.695	0.501	0.264	0.179	0.111	0.061
GV#13	1	0.207	0.175	0.128	0.113	0.097	0.079
GV#14	1	0.494	0.406	0.270	0.218	0.166	0.113
GV#17	2	0.0	0.0	0.0	0.0	0.0	0.000
		5.437	4.562	3.169	2.630	2.088	1.593
Taper Transition							
TP#1	1	0.731	0.537	0.313	0.248	0.187	0.127
TP#3	1	0.008	0.008	0.003	0.001	0.000	0.000
TP#4	2	0.019	-0.001	-0.001	0.000	0.001	0.000
TP#5	2	0.130	0.145	0.122	0.099	0.068	0.037
TP#6	6	0.004	0.029	0.026	0.013	0.005	0.001
		0.892	0.718	0.463	0.361	0.261	0.165
Position Monitor	45	2.721	2.057	1.133	0.708	0.610	0.270
Total		**41.47**	**34.67**	**15.68**	**11.13**	**8.13**	**5.38**

Table 3 Parasitic mode loss power of ring components. Bunch length s = 53.0 ps, average beam current I_0 = 50 mA.

Component	k (V/pC)	Power loss (W)
RF Cavity (Not including K_0=0.176)	0.319	498
Gate valve		
GV#1	0.143	223
GV#2	0.272	424
GV#5	0.267	416
GV#6	0.286	446
GV#7	0.434	677
GV#11	0.263	410
GV#14	0.218	340
Taper Transition		
TP#1	0.248	387

We determined the R_S and ω_c parameters in Eq. (6) by the method of least squares using the total loss parameters obtained in this study. The results are summarized bellow:

I. Ring impedance of the present PF Storage Ring

The values of the R_S and w_c parameters in Eq. (6), obtained from the total loss parameter (K) in Table 2 are,

$$\begin{aligned} R_S &= 8730\ \Omega, \\ \omega_c &= 27.6 \times 10^9\ \text{rad/s}, \\ |Z/n| &= 3.19\ \Omega. \end{aligned} \qquad (8)$$

The loss parameter as a function of the bunch length, ($K(\sigma)$), calculated by Eq. (6) with $R_S = 8730\ \Omega$ and $\omega_c = 27.6 \times 10^9$ rad/s is shown in Fig.19, as well as the measured results.

II. Ring impedance without bellows

The contribution of the bellows to the total loss parameter is very large at the short bunch region. It is interesting to estimate the ring impedance without all of the bellows. The value of the R_S and ω_c parameters in Eq. (6) obtained are as follows:

$$\begin{aligned} R_S &= 3322\ \Omega, \\ \omega_c &= 15.0 \times 10^9\ \text{rad/s}, \\ |Z/n| &= 2.23\ \Omega. \end{aligned} \qquad (9)$$

Broad band impedance $|Z/n|$ in this case is reduced to 70% of that of the present ring. The $K(\sigma)$ calculated for this case by Eq. (6) is shown in Fig.19.

III. Ring impedance without gate valves

If all the gate valve sections are smoothly RF screened, the value of parameters R_S and ω_c in this case are,

$$\begin{aligned} R_S &= 7801\ \Omega, \\ \omega_c &= 30.0 \times 10^9\ \text{rad/s}, \\ |Z/n| &= 2.62\ \Omega. \end{aligned} \qquad (10)$$

Broad band impedance |Z/n| is reduced to 82% of that of the present ring. The K(σ) calculated for this case by Eq. (6) is shown in Fig.19.

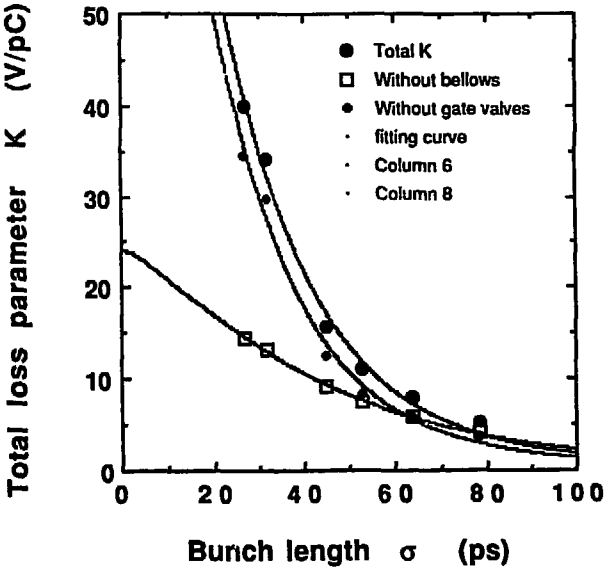

Fig. 19 Measured total loss parameter and that calculated using the broad band impedance model.

IV. Ring impedance without bellows and gate valves

If all the bellows and gate valve sections are RF screened, R_S and ω_C become as follows:

$$\begin{aligned} R_S &= 2136\ \Omega, \\ \omega_C &= 14.7 \times 10^9\ \text{rad/s}, \\ |Z/n| &= 1.46\ \Omega. \end{aligned} \qquad (11)$$

The broad band impedance |Z/n| in this case is reduced to 46% of that of the present ring.

The |Z/n| obtained in this study is 3.19 Ω, and since some components have been ignored, the value of |Z/n| would be slightly larger. The value of |Z/n| obtained by a study of bunch lengthening[13] under the single bunch operation is about 2 Ω. There is a small discrepancy between our result and the result given in ref. 13.

7. Conclusions

We measured and calculated loss parameters of the PF ring major components one by one, while excluding some, such as the SR ports and insertion devices. From these loss parameters, we evaluated the ring impedance, based on the broad band impedance model.

The PF ring impedance evaluated in this study is

$$|Z/n| = 3.19\ \Omega.$$

The ring impedance will be reduced to about one half of the present PF ring, if all bellows and gate valve sections are RF screened.

Concerning overheating problem under single bunch operation, this study indicates that most overheating takes place at the gate valves, and that improvements in the gate valves are necessary.

8. Acknowledgments

The authors would like to acknowledge Mr. Y. Takiyama and Prof. H. Kitamura who provided drafts of vacuum components and insertion devices.

We thank Mr. A. Mishina for his help in carrying out TBCI calculations.

T. Kiuchi also appreciates the hospitality of the Photon Factory during his stay at KEK.

References

1. M. Sands and J. Rees, SLAC-report PEP-95, August 1974.
2. P. B. Wilson, et al., IEEE Trans., NS-24, 1496, June 1977.
4. T. Weiland, Nucl. Instrum. Methods, 212, (1983), 13.
3. F. Caspers, IEEE Trans., NS-32,1914, October 1985.
5. M. Izawa, T. Kiuchi, S. Tokumoto, Y. Hori, S. Sakanaka, M. Kobayashi, and h. Kobayakawa, Rev. Sci. Instrum. 63(1992)366.
6. M. T. Menzel and H. K. Stokes, LA-UR-87-115, January 1987.
7. Y. Yamazaki and K. Takata, Proc. 3rd. Symp. Accele. Sci. Tech. (1980), p. 225.
8. T. Weiland, Nucl. Instrum. Methods, 216, (1983), 329.
9. PHOTON FACTORY ACTIVITY REPORT 1986, ISSN 0912-1803, 61, 1986.
10. J. N. Weaver, PEP-NOTE-342, January 1981.
11. J. L. Laclare, in Proc. CERN Accelerator School, General Accelerator Physics, Vol. II, Gif-sur-Yvette, Paris, France, 1984, CERN 85-19, p. 377.
12. P. B. Wilson, PEP-233, February 1977.
13. N. Nakamura, S. Sakanaka, K. Haga, M. Izawa, and T. Katsura, IEEE Proc. Part. Accele. Conf., 1(1991)440.

Appendix

Dimensions of Components.

R-Bellows#1 to #9

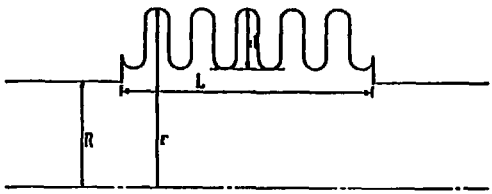

	R (mm)	r (mm)	L (mm)	d (mm)	No. of corugations
R-Bellows#1	75	80	45	10	5
R-Bellows#2	50	62	63	9.5	7
R-Bellows#3	50	67	70	15	8
R-Bellows#4	50	55	37.5	9	5
R-Bellows#5	32	40.5	45	8.5	4
R-Bellows#6	75	88	35	9	5
R-Bellows#7	75	80.5	58	9.5	5
R-Bellows#8	50	62	59	9.5	6
R-Bellows#9	55	63.5	27	9	2

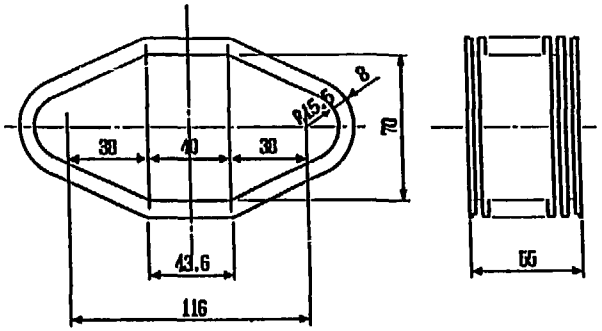

Q-bellows.

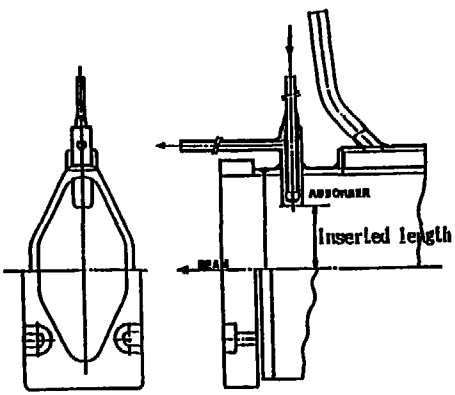

SR Absorber (Q-type)

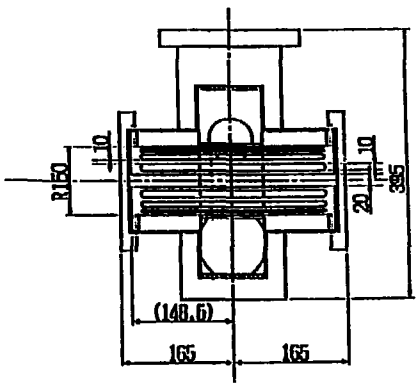

R-II Type (Pumping port)

GV#1

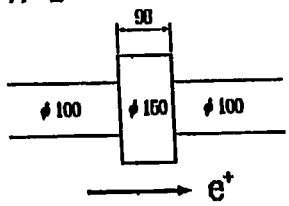

GV#2

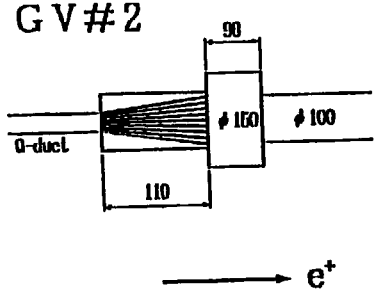

GV#3, 4

L=90 for GV#3
L=98 for GV#4

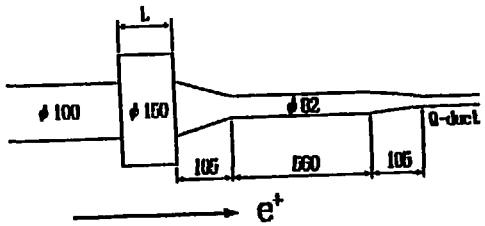

GV#5

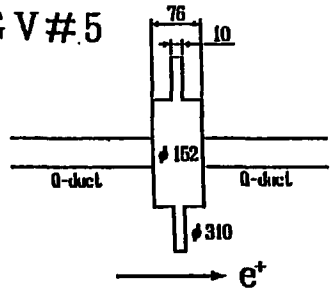
76
10
φ152
Q-duct
Q-duct
φ310
e+

GV#6

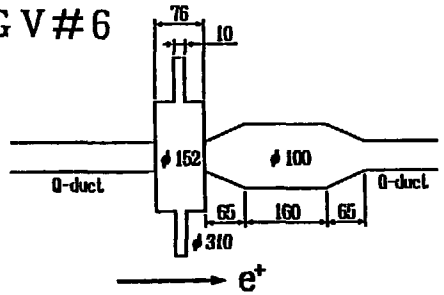
76
10
φ152
φ100
Q-duct
Q-duct
65
160
65
φ310
e+

GV#7

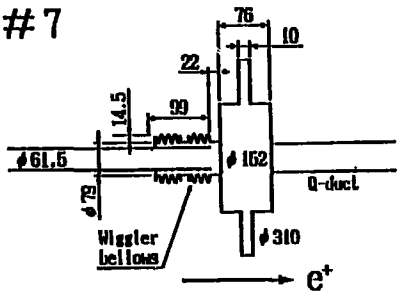
76
10
22
14.5
99
φ61.5
φ72
φ162
Q-duct
Wiggler bellows
φ310
e+

GV#11

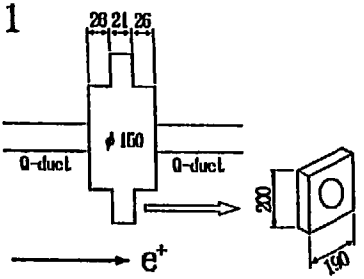

GV#12

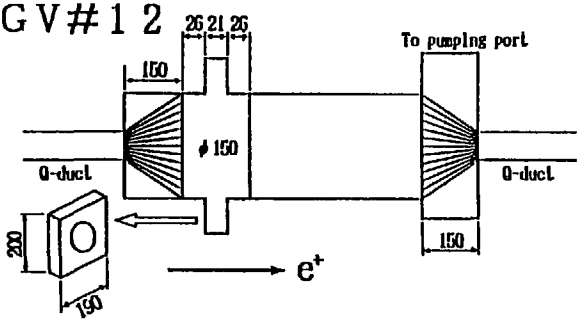

GV#13

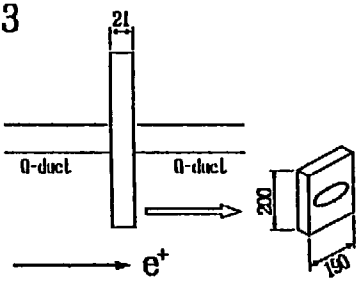

GV#14

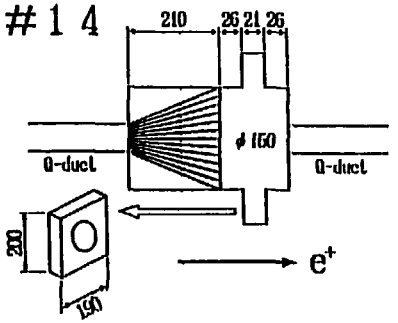

GV#11/#15

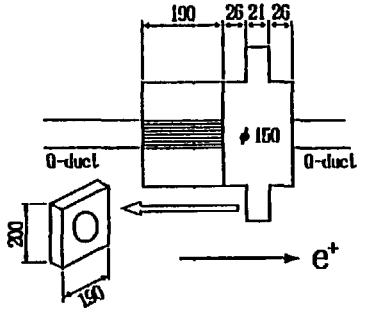

GV#16

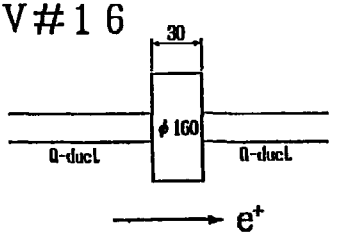

TP#1

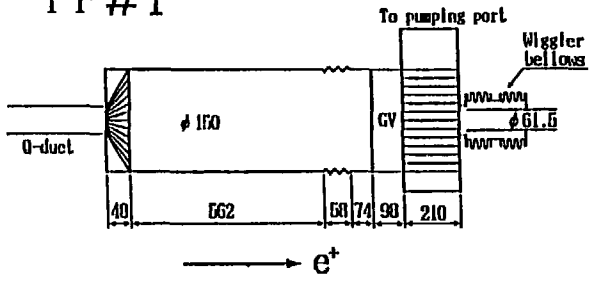

TP#3

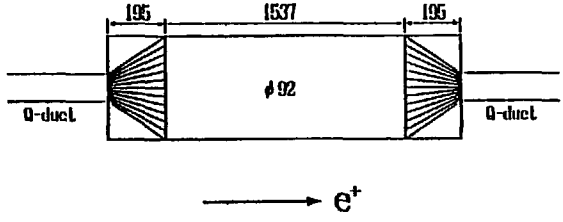

TP#4

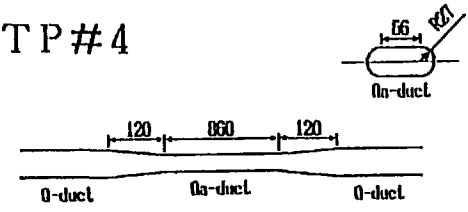

TP#5

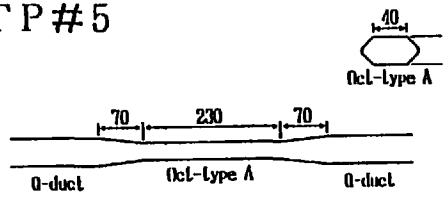

TP#6